Assessing Fracture Connectivity using Stable and Clumped Isotope Geochemistry of Calcite Cements

Kristina K. Sumner

A report prepared in partial fulfillment of
the requirements for the degree of

Master of Science
Earth and Space Sciences: Applied Geosciences

University of Washington

December, 2014

Project mentor:
Trenton C. Cladouhos, AltaRock Energy LLC

Internship coordinator:
Kathy Troost

Reading committee:
Katharine W. Huntington
Juliet G. Crider

MESSAGe Technical Report Number: 015

Abstract

Understanding flow path connectivity within a geothermal reservoir is a critical component for efficiently producing sustained flow rates of hot fluids from the subsurface. I present a new approach for characterizing subsurface fracture connectivity that combines petrographic and cold cathodoluminescence (CL) microscopy with stable isotope analysis ($\delta^{18}O$ and $\delta^{13}C$) and clumped isotope (Δ_{47}) thermometry of fracture-filling calcite cements from a geothermal reservoir in northern Nevada. Calcite cement samples were derived from both drill cuttings and core samples taken at various depths from wells within the geothermal field. CL microscopy of some fracture filling cements shows banding parallel to the fracture walls as well as brecciation, indicating that the cements are related to fracture opening and fault slip. Variations in trace element composition indicated by the luminescence patterns reflect variations in the composition and source of fluids moving through the fractures as they opened episodically. Calcite $\delta^{13}C$ and $\delta^{18}O$ results also show significant variation among the sampled cements, reflecting multiple generations of fluids and fracture connectivity. Clumped isotope analyses performed on a subset of the cements analyzed for conventional $\delta^{18}O$ and $\delta^{13}C$ mostly show calcite growth temperatures around 150°C—above the current ambient rock temperature, which indicates a common temperature trend for the geothermal reservoir. However, calcite cements sampled along faults located within the well field showed both cold (18.7°C) and hot (226.1°C) temperatures. The anomalously cool temperature found along the fault, using estimates from clumped isotope thermometry, suggests a possible connection to surface waters for the geothermal source fluids for this system. This information may indicate that some of the faults within the well field are transporting meteoric water from the surface to be heated at depth, which then is circulated through a complex network of fractures and other faults.

Table of Contents

List of Tables and Figures

Acknowledgements

I cannot begin to express my gratitude for the mentorship and guidance that I have received throughout this research: Trenton Cladouhos, Katharine Huntington, and Juliet Crider. To all of these incredibly talented individuals, I offer my sincerest appreciation for the learning opportunities that they have provided.

I also would like to thank Erin Camp and Matt Uddenberg for their unwavering support in the field – especially in 114°F weather. Additionally, this project would have never have made its deadlines, if it wasn't for Erin Camp's countless hours of lab assistance with sample prep. Also, I am incredibly grateful for the suggestions and insights from Geoffrey Garrison during this investigation, and for Mike Swyer's excellent fault models. Furthermore, the success of this project relied on the data processed within University of Washington's IsoLab, which is run by Andy Schauer. I would like to thank Andy for both his patience and wonderful instruction in showing a newbie how to be proficient on these hi-tech and sometimes complicated machines.

Finally, this project would not have been possible without the generous research grant that I received from AltaRock Energy. Thank you!

1 Introduction

Geothermal systems extract heat energy from the earth by moving hot fluids through a deep, complex fracture network (Barbier, 2002). Geothermal fields are dynamic systems that are continually changing and evolving through time (Lowell *et al.*, 1993; Bruel, 2002; Yasuhara *et al.*, 2006). Because of this dynamic nature, these changes demand regular evaluation and adjustments to receive maximum beneficial energy extraction results. However, before field optimization can be achieved, an in-depth understanding of fluid pathways is crucial (Horne and Rodriquiez, 1983; Sheridan *et al.*, 2003). Here, I report on a new integrated approach that uses cold-cathodoluminescence (CL), stable isotope analyses of $\delta^{18}O$ and $\delta^{13}C$, and clumped isotope geothermometry (Δ_{47}) to evaluate precipitated calcite cements deposited by geothermal fluids along the reservoir fracture network. Prior stable and clumped isotope research along faults has shown promising results in the ability to determine the thermal evolution of these structures and their source fluids (Bergman *et al.*, 2013; Swanson *et al.*, 2012). The results of this research may benefit both geothermal resource managers and developers in future reservoir characterization.

1.1 Study Area

Blue Mountain is an eastward tilted fault block located within the Basin and Range Province in northern Nevada. Blue Mountain is positioned on the north-central end of the of the Luning-Fencemaker fold-and-thrust belt (Wyld, 2002) (Figure 1). There are three predominant, stratigraphic units of Triassic age found within this area, which are metamorphosed shales of phyllite and black slate, interbeds of metasandstone, and rare (3-4%) occurrences of limestone (Wyld, 2002). Deformation within these units show two strain regimes that reflect northwest-southeast crustal shortening followed by low-grade metamorphism (phase 1), and minor northeast-southwest shortening (phase 2)(Wyld, 2002). Locally, within the Blue Mountain geothermal field, there are multiple fault zones located on the western, northwestern, and southwestern edges. These faults merge

within the area of the geothermal field on the western flanks of Blue Mountain (Faulds and Melosh, 2008)(Figure 2). The fault-controlled, geothermal site has 5 production wells located in the center of the field with 9 injectors along the perimeter, and 4 idle wells (Figure 2). The Blue Mountain geothermal site is currently under investigation by a resource management group that aims to optimize the production and injections program through determination of optimal well stimulation targets.

1.2 Scope of Work

My research seeks to apply a multi-tiered approach in using: cold-cathodoluminescence (CL), stable isotope analyses of $\delta^{18}O$ and $\delta^{13}C$, and clumped isotope geothermometry (Δ_{47}) of calcite cements, to aid in subsurface connectivity characterization between the wells within the geothermal well field, and provide insight into the fluid sources for the system. Specifically my investigation will: 1) correlate veins between targeted wells by analyzing the stable isotope signature found in the precipitated calcite deposited within the subsurface fracture network, relying on the $\delta^{18}O$ and $\delta^{13}C$ composition ratios of the calcite samples taken from each well within the geothermal field, 2) obtain paleofluid temperatures from the calcite deposits within the veins using clumped isotope thermometry, which does not require knowledge of the isotopic composition of the paleofluid in which the calcite was precipitated from (Ghosh *et al.*, 2006), 3) determine the water-source for this system (i.e. is the water meteoric or does it have a deeper mixing signature) using temperatures and $\delta^{18}O_{H2O}$ values calculated from the temperature and $\delta^{18}O_{calcite}$ value from stable isotope geochemistry of calcite deposits, which reflect temperatures of calcite growth along fluid pathways, and 4) identify multiple generations of calcite precipitation using cold-cathode cathodoluminescence (CL) microscopy on the calcite deposits, where trace elements within the calcite crystal lattice luminesce when stimulated by an electron beam and show changes in crystal growth composition (Boggs and Krinsley, 2006).

2 Methods

This section will describe the office review conducted before entering the field site, the sample collection methods used while in the field, and the lab procedures used to characterize calcite taken from rock cores and drill cutting from the Blue Mountain geothermal site.

2.1 Office Review

Before collecting calcite samples, it was imperative to target the calcite deposits to maximize the limited time at the field site. To achieve this, I reviewed several, internal AltaRock Energy documents concerning well drill cuttings and core. The samples to be collected were primarily from drill cuttings; however, there were two wells (DB-1 and DB-2) that had continuous core available for the investigation.

2.1.1 Pre-field Investigation

A list of twenty wells that consisted of current producers and injectors, future producers, and stimulation targets was provided by AltaRock Energy for evaluation. The well list was prioritized by AltaRock Energy to reflect those wells and well depths most important for development of a future optimization project. From this list, I chose at least one top priority well from each of the AltaRock Energy categories (i.e. producers, injectors, etc.), and selected several secondary priority wells to investigate. The wells chosen from the categorized priority list were cross referenced to their respective well logs, which were also provided by AltaRock Energy, to determine the availability of calcite at the depths of interest. The well logs provided information pertaining to types of minerals found in drill cuttings, including calcite, and the percentages of each mineral found at ten foot depth intervals. The target percentages of calcite were “Common” (4%-7%), “Abundant” (7%-10%), and greater than “Abundant” (>10%). If the desired depth interval for a given well did not have calcite noted in the well log or if there was rare (<1%) to trace (1%-4%) calcite found, I then looked for adjacent depth intervals that reflected greater abundances of calcite. During this evaluation, I also considered areas within the well logs that noted drilling mud losses or fault gouge. These

features may indicate the presence of faults, and/or mark the area that a given well has intersected a large fluid conduit. Locations at which calcite was found adjacent to these fault depth intervals were also marked as depths of interest for lab analyses.

The samples from the two available cores (DB-1 and DB-2) were evaluated based on their core logs. Unfortunately, the information within the core logs was sparse and did not indicate any findings of calcite. Because of the prevalence of calcite found within the other wells throughout the well field, it was determined that calcite might have been overlooked during the initial logging of these cores. Since there was no prior information pertaining to calcite, I found it necessary to test these cores at their storage facility for calcite using a dropper bottle of hydrochloric acid (HCl).

Once the evaluation of the twenty wells within the field site was finished, I was able to narrow the focus to eleven wells of interest that contained calcite. This focus predominantly reflects the wells that AltaRock Energy was most interested in for gleaning more information on the interconnectedness between these wells for future stimulation projects. The wells that were selected for samples analyses are as follows: 26A-14, 34-23, 38-14, 41-27, 58-15, 61-22, 86-22, 89-11, 91-15, DB-1, and DB-2 (Figure 2).

2.2 Field Methods

After the target intervals were identified, calcite samples were collected from archived drill core and cuttings held onsite in Nevada. While onsite, the following equipment was used: HCl acid bottles, hand lenses, binocular microscopes, folding table, sampling knives, sun tent, and water jugs. A description of our calcite sampling methods is provided within the next section, 2.2.1.

2.2.1 Field Sampling Methods

The drill cuttings were located within a storage facility in northern Nevada. The cuttings were contained in labeled sample bags that were stored in marked boxes, which were divided by well and further subdivided by well depth. This

categorization of the wells by depths made finding the targeted sample bags fairly easy. However, the samples had not been cleaned of the drilling mud during the drilling process, and it was impossible to evaluate calcite content in the field. Dried drilling mud creates a solid cement around the cuttings, which is not easily removed without detergent and a lot of water. Because of this situation, I had to trust that the drill logs were accurate in determining percentage of calcite for each sample. It is worth noting that the targeted well depths for well number 34-23 were not found within the storage facility and there were only samples that had trace amounts of calcite present. The sparse presence of calcite for well 34-23 is reflected in the limited samples shown for this well in the results section of this report.

The cores for wells DB-1 and DB-2 were stored in core boxes located at the geothermal field site. The core logs for DB-1 and DB-2 showed very little to no calcite, so onsite testing was conducted. Approximately, 5,900 feet of core was processed in the field using hydrochloric acid (HCl) to determine calcite content. Each core box contained ten feet of core. While in the field, each core box was opened and the core was visually inspected for calcite. HCl was also applied to each occurrence to confirm the presence of calcite. The samples that tested positive for calcite were cataloged by well and depth, and then placed in plastic bags for transport. Each core taken was later photographed to add to the cataloged sample core index.

2.3 Laboratory Methods

Core and drill cutting samples collected in the field were brought back to the University of Washington to prepare for laboratory analyses. The core was catalogued and seven sections of core, from both DB-1 and DB-2, were selected and cut into smaller pieces using a rock saw. Thin sections from the core pieces were created for cold cathodoluminescence (CL) microscopy, which is described below. The mud-cemented cuttings were washed using water and sometimes dish washing detergent. During the washing, the cuttings were also wet sieved and separated into size fractions to make finding calcite easier. The cuttings were then left out to air dry for several days. Once the cuttings were dried and placed into plastic sample bags

for storage, calcite pieces were picked out from the larger sized fractions using tweezers under a microscope. Under the microscope, a drop of HCl and a drop of deionized (DI) water were placed adjacent to each other on a glass slide. Each small cutting that when visually inspected resembled calcite, was dipped into HCl to determine the relative calcite content. This is a qualitative test that determines whether the small piece of rock, under the microscope, contains enough calcite for isotopic analysis. Once a piece of calcite was positively identified through its reaction with HCl, the small chip was placed in the drop of DI water to stop the reaction and then dried. This process was carried out for all of the drill cuttings selected for further evaluation.

2.3.1 Cold Cathodoluminescence (CL) Microscopy

The core samples that were selected for CL were cut down into smaller pieces. From DB-2 samples were selected at depths of 1583', 2806', 3456', and 4607'. The depth of the DB-2 well is 5,000 feet and the core samples were chosen at the particular depths given because of the predominance of calcite found at these locations, which were at approximately 1000 foot intervals. The depth of the DB-1 well is 2,205 feet, and this core had less calcite spaced throughout the core. Most of the calcite found in DB-1 was within relatively narrow zones that were fairly close to each other. From DB-1, calcite zones were sampled at depths of 1723', 1770', 1960', and 2203'. However, one of the core samples from DB-1 (depth 2203') was found to not have any calcite along the fracture and was discarded from further analysis. The core was cut perpendicular to fracture plane to fit onto petrographic slides. These slides were used to create high-polished thin sections for CL analyses, using a Technosyn Luminoscope to visually characterize the carbonate cements within the thin section samples.

Cold cathodoluminescence microscopy shows changes in chemical composition by concentrating a stream of electrons on the high-polished, thin sections (De Abajo, 2010). The bombardment of electrons either excites impurities within the calcite crystal lattice or the impurities absorb the induced energy stream (Boggs and Krinsley, 2006). When an atom is excited through electron stimulation, it

causes the atom to release a photon of light within the visible spectrum. After the release of the photon, the atom returns to its lower energy state (Boggs and Krinsley, 2006). These excited atoms are known as activators (Machel, 1985; Boggs and Krinsley, 2006). If the atoms within the crystal lattice absorb energy and emit no photons, then they are known as quenchers (Machel, 1985; Boggs and Krinsley, 2006). The two main impurities for calcite that can be detected through CL are Mn^{2+} and Fe^{2+}, which are respectively an activator and a quencher (Machel, 1985; Boggs and Krinsley, 2006). The change in concentration of these atoms (Mn^{2+} and Fe^{2+}) within the calcite cement is reflected as changes in the intensity and color observed during electron stimulation (Machel, 1985). Colors that may be observed during CL are yellowish-orange to red (contribution from activators) with lighter or darker hues (contribution from quenchers). Overall, color changes observed within the calcite sample correlate to changes in fluid composition (Boggs and Krinsley, 2006).

2.3.2 Stable Isotope Analysis

Before conducting a clumped isotope analysis, the carbon and oxygen isotopic compositions of the prepared samples were measured (i.e. their $\delta^{18}O$ and $\delta^{13}C$ values). Seventy-two samples from eleven wells, which included both drill cuttings and the core, were analyzed (Table 1). For each given well and well depth, two separate calcite samples were pulverized with an agate mortar and pestle. The decision to pick two samples from each well depth transpired from the results of the CL analyses of core samples, which showed at least two generations of calcite (discussed below). The pulverized carbonate samples (0.02 – 0.12mg) were then processed at the University of Washington's IsoLab using a Kiel III carbonate device coupled to a Finnigan Delta Plus mass spectrometer. The mass spectrometer is a device that subjects ionized CO_2 gas to a magnetic field, which deflects each ion in the CO_2 molecule according to its mass-to-charge ratio (Sparkman, 2000). The device then detects masses 44, 45, and 46, which then calculates the abundances of $\delta^{16}O$, $\delta^{18}O$, $\delta 12C$ and $\delta^{13}C$ of the sample gas, and compares these values to those found in a standardized reference gas to get the $\delta^{18}O/\ \delta^{16}O$ and $\delta^{13}C/\ \delta^{12}C$ ratios. All $\delta^{18}O$ and $\delta^{13}C$ values are referenced to Vienna Peedee Belemnite (VPDB), which is an

international standard that carbon and oxygen isotopes are measured relative to (Slater *et al.*, 2001).

From the drill cuttings, two samples were selected from each depth interval per sampled well. The two samples were selected based on visual differences in the characteristics of the calcite pieces (i.e. color and texture). In addition, two core samples from DB-1 (1723' and 1770') were analyzed using CL and were set aside for more fine-scaled stable isotope evaluation. These two samples showed at least two generations of calcite, and each generation was separately targeted within the sample by using a high precision micro mill. The micro mill was used to drill out a sample from each of the two different CL bands to see if isotopic changes could be detected. The micro milled core samples have been prepared for future stable isotope analysis.

2.3.3 Clumped Isotope (Δ_{47}) Analysis

The Δ_{47} analysis is based on the tendency of heavy carbon and oxygen isotopes of calcium carbonate ($CaCO_3$) to preferentially "clump" together, which is influenced by the temperature at which the calcite precipitated (Schauble *et al.*, 2006; Ghosh *et al.*, 2006; Eiler, 2007). These are known as isotopologues, which are molecules that have the same chemical composition, but differ in their isotopic composition (Eiler, 2007). Clumped isotope geochemistry evaluates the amount of "clumping" found within gaseous CO_2, which is the resultant product of acid digestion of calcite. The isotopologue of the CO_2 gas that is evaluated for this study has an ionic mass of 47, which correlates to the ^{13}C-^{18}O-^{16}O species. In addition, this analysis also measures masses 44, 45, and 46, which again calculates both the $\delta^{18}O$ and the $\delta^{13}C$ of the sample to give further verification of the stable isotope ratios. Furthermore, the clumped isotope paleothermometer is unique in that it does not rely on the composition of the fluid in which the carbonate cement formed from (Ghosh *et al.*, 2006). This one aspect is extremely important for our study, because the paleo-composition of the subsurface fluids, within the Blue Mountain geothermal field, is not independently known. However, once the temperature and the $\delta^{18}O_{calcite}$ is known, I will be able to calculate the $\delta^{18}O_{H2O}$ using an equation

published by Kim & O'Neil (Kim and O'Neil, 2007). All $\delta^{18}O_{H2O}$ values are referenced to Vienna Standard Mean Ocean Water (VSMOW), which is an international water standard that defines oxygen isotopic compositions (Coplen, 1995).

A subset of ten samples was selected for the clumped isotope Δ_{47} study. The wells selected reflect six samples from cuttings and four samples from the core, of which only one sample is from the core DB-1 (Table 1). This subset was determined by organizing the data from the $\delta^{18}O$ and $\delta^{13}C$ analyses (Figure 4). My subset selection reflects high and low value combinations of $\delta^{18}O$ and $\delta^{13}C$ seen throughout the data.

To prepare samples for clumped isotope measurements, 8-12 mg of each sample were powdered using an agate mortar and pestle, and then pre-treated using 3 percent solution of hydrogen peroxide (H_2O_2) for 45 minutes to remove organic material (Bergman *et al.*, 2013). Unlike the stable isotope analysis, the calcite for each of the ten samples was combined and crushed into a single sample. Following the cleaning procedure, the prepared samples were digested in a common phosphoric acid bath (H_2PO_4) held at 90 °C to produce CO_2, which then passed through multiple cryogenic traps to create a purified CO_2 sample (Passey *et al.*, 2012). Finally, the CO_2 gasses were analyzed in a mass spectrometer (Thermo MAT253) at the University of Washington's IsoLab, which calculated the amount of isotopologues of mass-47 in each sample (Huntington *et al.*, 2009). This process was replicated at least twice for each sample. The Δ_{47} values reported in Table 1 are given in the absolute reference frame, which is a standardized reference frame in which sample CO_2 isotopologue values are referenced to values measured for CO_2 equilibrated at known temperatures (ARF; Dennis *et al*., 2011).

3 Results

Laboratory results from each of the analytical procedures are described in detail below. I have processed and analyzed seven samples for CL, seventy-two samples for stable isotope analyses, and a subset of ten samples for clumped isotope thermometry. Many of the findings from the various studies are preliminary.

3.1 Cold Cathodoluminescence (CL) Microscopy

Thin sections from the seven core samples were evaluated using transmitted and polarized light, as well as cold cathodoluminescence (CL) microscopy. Calcite from the seven core samples was found to occur as fracture fill that created a veneer on top of a layer of fine quartz crystals (i.e. druzy quartz). This layering indicates that the quartz-rich fluid was first to circulate through this system and is seen as the primary filler within the void spaces and fractures. The calcite within our samples is shown in CL images as a reddish orange luminescent color (Figures 5-8). The thin sections from both cores exhibit this color spectrum. However, there are two thin sections from the DB-1 core (depths 1723' and 1770') that show banding (Figure 9). Calcite twinning is also observed throughout both the polarized and transmitted light images (Figures 5-8).

3.2 Stable Isotope Analysis

For this evaluation the $\delta^{18}O$ and $\delta^{13}C$ content of my carbonate samples was analyzed to establish compositional variations between each well using calcite samples derived from both drill cuttings and core. The seventy-two sample were plotted on both a "well-depth" versus $\delta^{18}O$ and $\delta^{13}C$ (VPDB), and a $\delta^{18}O$ versus $\delta^{13}C$ (VPDB) graph to look for relationships between the $\delta^{18}O$ and $\delta^{13}C$ datasets (Figures 3 and 4) (Table 1). The seventy-two samples showed to have a wide range of $\delta^{18}O_{Carbonate}$ values from -19.4 ‰ to -35.8‰ (VPDB), which had standard errors no greater than +/- 0.1‰ (Table 1).

In additions to these seventy-two carbonate sample values, the subset of ten samples analyzed for clumped isotope thermometry and whose $\delta^{18}O$ and $\delta^{13}C$ values were also determined, reflected this broad range of values for the carbonate samples. The $\delta^{18}O_{Carbonate}$ values for the subset ranged from -13.2‰ to -33.5‰ (VPDB) with a measured standard error generally less than +/- 0.1‰ (Table 1).

The $\delta^{13}C$ stable isotopic values for the seventy-two samples varied from -5.1‰ to -12.3‰, +/- 0.1‰ (VPDB) (Figures 3 and 4)(Table 1). The subset of ten samples that were analyzed for clumped isotope thermometry had similar ranges of

$\delta^{13}C$ values, which are -7.2‰ to -13.4‰, and had standard errors no greater than +/- 0.2‰ (VPDB)(Table 1).

3.3 Clumped Isotope (Δ_{47}) Analysis

The stable isotope evaluation shows that the isotopic composition of the calcite is variable. The subset of ten samples (Figure 10), from both drill cuttings and core, was chosen to further investigate these ranges and determine the cause of the variations seen in the $\delta^{18}O$ and $\delta^{13}C$ values through a clumped isotope Δ_{47} analysis (i.e. is temperature effecting the variation in $\delta^{18}O$ and $\delta^{13}C$ values). Preliminary findings show a narrow range of temperatures from 124°C to 162°C with errors no greater than +/- 31°C, which is above host rock temperature for the sampled depths (Table 1). However, there are two samples taken from wells 26A14-2600 and 2-3456, which have anomalous temperature values of 19°C and 226°C respectively (Table 1). The Δ_{47} values found from our clumped isotope thermometry analyses range from 0.393 to 0.711 with errors less than +/- .032.

As stated in section 2.3.3, the isotopic ratio for the water in which the calcite precipitated could be calculated once temperature and $\delta^{18}O_{Carbonate}$ of the samples were known (Kim and O'neil, 1997). The subset of ten samples analyzed for clumped isotope thermometry had calculated $\delta^{18}O_{H2O}$ (VSMOW) values that ranged from 1‰ to -13‰ (VSMOW), with calculated standard errors less than +/- 3‰ (Figure 4) (Table 1).

4 Discussion

4.1 Cold Cathodoluminescence (CL) Microscopy

The four samples from core DB-2 that were examined using CL microscopy did not show variations in the trace element composition of the calcite. Two samples from core DB-1 showed distinct compositional changes in the form of banding, which can be seen as slight differences in luminescence between each growth layer (Figure 9). The banding is most likely from fracture growth bands and marks the

growth of the fracture and calcite cement fill (e.g. Sippel and Glover, 1965; Morad *et al,* 2012). Fracture opening and fill does not necessarily happen at the same location for every open and fill event (David Budd, Professor of Geological Sciences, University of Colorado Boulder, written communication, 2014). For example, a fracture may open with calcite cements precipitating along the middle of the fracture. The next fracture growth may open a void along the outside wall of the fracture, which allows for calcite growth along the outside of the previous calcite deposit instead of growing inward.

Overall, these findings show that the composition of the fluids within the reservoir has changed over time and that there are at least two compositional changes. Additionally, the banding reflects movement within the geothermal system and aperture growth along fractures.

4.2 Stable Isotope Analysis

Variations in $\delta^{18}O$ and $\delta^{13}C$ can either be from changes in temperatures, fluid composition, or both (Zheng and Hoefs, 1993). There is such a broad range of $\delta^{18}O$ values that further Δ_{47} analysis is needed to help constrain which variable (i.e. temperature or fluid composition) has the greatest influence on the stable isotope values, which is discussed below in section 4.3.

The $\delta^{18}O_{carbonate}$ is largely variable throughout the geothermal field and shows depletion of $\delta^{18}O$ within the calcite cements. Large ranges in $\delta^{18}O$ and $\delta^{13}C$ greater than a 6‰ (VPDB) spread in values represents significant interactions between the geothermal fluid and the reservoir rock (Maskenskaya, 2014). The range of $\delta^{18}O_{carbonate}$ values for the Blue Mountain geothermal system is 16.5‰ (VPDB), which demonstrates interaction of the source fluid with the reservoir rock. Additionally, other research has also found that convective, inorganic hydrothermal fluids tend to be highly depleted in both $\delta^{18}O$ and $\delta^{13}C$ from considerable interactions with the host-rock in geothermal fields (Drake and Tullborg, 2009).

The reported ranges of $\delta^{13}C_{carbonate}$ values for our geothermal system also reflect carbon depletion in the reservoir that can be a result of many factors. It has been found that epithermal deposits, inorganic carbon from host-rock, a Permian-

Triassic pyrite carbon isotope excursion, or reworked hydrothermal calcite can all relate to the negative values for the measured $\delta^{13}C_{carbonate}$ for this system (Haas *et al.*, 2006; Bottomley and Veizer, 1991; Clark and Fritz, 1997; Meinert, 1992). Currently, there is no indication of which contributing factor has the greatest influence on the $\delta^{13}C_{carbonate}$ depletion for this geothermal system.

4.3 Clumped Isotope Analysis

From the preliminary results, it does not appear that $\delta^{18}O_{H2O}$ of our geothermal fluids and the $\delta^{13}C_{carbonate}$ are linked and no clear relationship between the two can be determined (Figure 11). Additionally, the preliminary results show that neither the $\delta^{18}O_{H2O}$ nor $\delta^{13}C_{carbonate}$ are dependent on temperature (Figure 12). This confirms that the variations of stable isotope values are most likely a reflection in changes of fluid composition rather than temperature.

Temperatures within the geothermal field during precipitation of our calcite samples were similar to current reservoir temperature of approximately 167°C. There are also two temperature extremes in our sample subset. One of the data points (26A14-2600') shows a cool precipitation temperature. This data point also correlates to a significant drilling-mud loss zone and is most likely a fault. The cool precipitation temperature could indicate a meteoric recharge path where the fault is funneling cooler surface waters down into the reservoir. The other fault related sample (DB2-720') is within temperature range of fracture fill cements. Except for the two anomalous temperature data points, the temperature within the reservoir stays close to approximately 150°C. The consistency of the reservoir temperature seen throughout the other eight wells is related to convective cycling of fluids through the system.

The variability of $\delta^{18}O_{H2O}$ values calculated from the measured temperatures seem to be quite common for connate and formation water in hydrothermal systems that are located in sedimentary basins. These waters have $\delta^{18}O_{H2O}$ ranges of -20‰ to 10‰ (VSMOW) and tend to reflect meteoric $\delta^{18}O_{H2O}$ values (Pirajno, 2008), which is consistent with the derived $\delta^{18}O_{H2O}$ values for this geothermal system. Furthermore, a 2002 study of $\delta^{18}O$ values for meteoric waters within the vicinity of

the Blue Mountain geothermal field showed a wide range of values. This study evaluated monthly $\delta^{18}O$ for three consecutive water years (1991through 1993), and found meteoric $\delta^{18}O_{H2O}$ values to range from 13.0‰ to -21.9‰ (VSMOW) (Friedman *et al,* 2002), which also agrees with the calculated $\delta^{18}O_{H2O}$ results.

The relationship within this dataset that is most interesting is the $\delta^{18}O_{H2O}$, $\delta^{13}C_{carbonate}$, and Temperature versus depth (Figure 13). At depth intervals between 2,000 feet and 3,500 feet, there seems to be a shift in both the stable isotope values and the temperature. One of these values within this depth interval is related to a fault; however, the other value (DB2-3456') does not correspond to any fault related information for that depth. Additionally, both of the temperature extremes seen in our sample subset are within this depth range.

4.4 Future Work

Carbonate samples have been extracted from the two thin sections where banding was observed in core DB-1. Each band was sampled using a micro mill. The samples will be analyzed for their $\delta^{18}O$ and $\delta^{13}C$ composition on a mass spectrometer. This analysis will provide information on compositional changes related to the banding.

One of the intentions of this study was to also evaluate whether it would be possible to look at a data point on the graph of "well-depth versus $\delta^{18}O$ and $\delta^{13}C$" (Figure 3), and be able to say that two independent points on the graph may be related to each other based on their $\delta^{18}O$ values (i.e. two separate data points are related because of their similar $\delta^{18}O$ compositional values). Because each of the data points represents a well, then similar $\delta^{18}O$ values plotted on the graph could represent connections and/or relationships between other wells of the same $\delta^{18}O$ composition. This information would enable geothermal resource managers to evaluate the connectivity between wells within the reservoir to determine future stimulation projects. However, to be able to do this, more data will need to be evaluated to conclusively determine that the variations in $\delta^{18}O$ are based solely on composition. Ten more data points will be added to the clumped isotope analysis to ascertain that the $\delta^{18}O$ variations are not influenced by temperature.

5.0 Summary

This research shows that this multistage approach using cold cathodoluminescence (CL) microscopy with stable isotope analysis ($\delta^{18}O$ and $\delta^{13}C$) and clumped isotope (Δ_{47}) thermometry of fracture-filling calcite cements can aid in the characterization of a geothermal reservoir. This project was able to show that throughout the reservoir at various depths the temperature is consistent except near the fault zones. These changes in temperatures seen at the fault zones indicate heterogeneity of fluid flow driven by the faults. For example, correspondence between a cold-temperature cement and fault gouge suggests that fluids circulating within the fracture networks could be sourced from meteoric waters that channeled down through the faults to be heated at depth. The preliminary Δ_{47} data indicates that our $\delta^{18}O$ and $\delta^{13}C$ values are not dependent on temperature, and the variations of stable isotope values are a reflection in changes of fluid composition. However, more data will need to be evaluated to clearly establish this.

6 References Cited

Barbier, E., 2002. Geothermal Energy Technology and Current Status: An Overview. Renewable and Sustainable Energy Reviews, Vol. 6, No.1, pp. 3-65.

Bergman, S. C., Huntington, K. W., Crider, J. G., 2013. Tracing Paleofluid Sources using Clumped Isotope Thermometry of Diagenetic Cements along the Moab Fault, Utah. American Journal of Science, Vol. 313, No. 5, pp. 490-515.

Boggs, S., Krinsley, D., 2006. Application of Cathodoluminescence Imaging to the Study of Sedimentary Rocks. Cambridge University Press.

Bottomley, D. J., Veizer, J., 1992. The Nature of Groundwater Flow in Fractured Rock: Evidence from the Isotopic and Chemical Evolution of Recrystallized Fracture Calcites from the Canadian Precambrian Shield. Geochimica et Cosmochimica acta, Vol. 56, No. 1, pp. 369-388.

Bruel, D., 2002. Impact of Induced Thermal Stresses during Circulation Tests in an Engineered Fractured Geothermal Reservoir: Example of the Soultz-Sous-Forets European Hot Fractured Rock Geothermal Project, Rhine Graben, France. Oil & Gas Science and Technology, Vol. 57, No. 5, pp. 459-470.

Clark, I. D., and Fritz, P., 1997. Environmental Isotopes in Hydrogeology. CRC Press.

Coplen, T. B., 1995. Reporting of Stable Carbon, Hydrogen, and Oxygen Isotopic Abundances. Reference and Intercomparison Materials for Stable Isotopes of Light Elements, 825, 31-34.

De Abajo, F. G., 2010. Optical Excitations in Electron Microscopy. Reviews of Modern Physics, Vol. 82, No. 1, pp. 209.

Dennis, K. J., Affek, H. P., Passey, B. H., Schrag, D. P., Eiler, J. M., 2011. Defining an Absolute Reference Frame for 'Clumped'Isotope Studies of CO_2. Geochimica et Cosmochimica Acta, Vol. 75, No. 22, pp. 7117-7131.

Drake H, Tullborg EL, 2009. Paleohydrogeological Events Recorded by Stable Isotopes, Fluid Inclusions and Trace Elements in Fracture Minerals in Crystalline Rock, Simpevarp Area, SE Sweden. Applied Geochemistry, Vol. 24, pp. 715–32

Eiler, J.M., 2007. "Clumped-Isotope" Geochemistry – The Study of Naturally-Occurring, Multiply-Substituted Isotopologues. Earth and Planetary Science Letters, Vol. 262, No. 3-4, pp. 309-327.

Faulds, J.E., Melosh, G., 2008. A Preliminary Structural Model for the Blue Mountain Geothermal Field, Humboldt County, Nevada. GRC Transactions, Vol. 32, pp. 273-278.

Friedman, I., Harris, J. M., Smith, G. I., Johnson, C. A., 2002. Stable Isotope Composition of Waters in the Great Basin, United States 1. Air-mass Trajectories. Journal of Geophysical Research: Atmospheres (1984–2012), Vol. 107, No. D19, ACL-14.

Gosh et al., 2006. ^{13}C-^{18}O Bonds in Carbonate Minerals: A New Kind of Paleothermometer. Geochimica et Cosmochimica Acta, Vol. 70, No. 5, pp. 1439-1456.

Haas, J., Demény, A., Hips, K., Vennemann, T. W., 2006. Carbon Isotope Excursions and Microfacies Changes in Marine Permian–Triassic Boundary Sections in Hungary. Palaeogeography, Palaeoclimatology, Palaeoecology. Vol. 237, No. 2, pp. 160-181.

Henkes, G.A., et al., 2013. Carbonate Clumped Isotope Compositions of Modern Marine Mollusk and Brachiopod Shells. Geochimica et Cosmochimica Acta, Vol. 106, pp. 307-325.

Horne, R. N., Rodriguez, F., 1983. Dispersion in tracer flow in fractured geothermal systems. Geophysical Research Letters, Vol. 10, No.4, pp. 289-292.

Huntington, K. W., Eiler, J. M., Affek, H. P., Guo, W., Bonifacie, M., Yeung, L.Y., Thiagarajan, N., Passey, B., Tripati, A., Daeron, M., Came, R., 2009. Methods and Limitations of 'Clumped'CO_2 Isotope (Δ_{47}) Analysis by Gas-Source Isotope Ratio Mass Spectrometry. Journal of Mass Spectrometry, Vol. 44, No. 9, 1318-1329.

Kim, S. T., O'Neil, J. R., 1997. Equilibrium and Nonequilibrium Oxygen Isotope Effects in Synthetic Carbonates. Geochimica et Cosmochimica Acta, Vol. 61, No.16, pp. 3461-3475.

Lowell, R. P., Van Cappellen, P., Germanovich, L. N., 1993. Silica Precipitation in Fractures and the Evolution of Permeability in Hydrothermal Upflow Zones. Science, Vol. 260, No.5105, pp. 192-194.

Machel, H. G., 1985. Cathodoluminescence in Calcite and Dolomite and its Chemical Interpretation. Geoscience Canada, Vol. 12, No. 4, pp. 139-147.

Maskenskaya, O. M., Drake, H., Broman, C., Hogmalm, J. K., Czuppon, G., Åström, M. E., 2014. Source and Character of Syntaxial Hydrothermal Calcite Veins in Paleoproterozoic Crystalline Rocks Revealed by Fine- scale Investigations. Geofluids, Vol. 14, No. 4, pp. 495-511.

Meinert, L. D., 1992. Skarns and Skarn Deposits. Geoscience Canada, Vol. 19, No. 4.

Morad S., Ketzer, M., deRos, L.F., 2012. Linking Diagenesis to Sequence Stratigraphy. John Wiley & Sons, West Sussex, UK.

Passey, B. H., Henkes, G. A., 2012. Carbonate Clumped Isotope Bond Reordering and Geospeedometry. Earth and Planetary Science Letters, Vol. 351, pp. 223-236.

Pirajno, F., 2008. Hydrothermal processes and mineral systems. Springer.

Schauble, et al., 2006. Preferential Formation of ^{13}C-^{18}O Bonds in Carbonate Minerals, Estimated using First-Principles Lattice Dynamics. Geochimica et Cosmochimica Acta, Vol. 70, No. 10, pp. 2510-2529.

Sheridan, J., Kovac, K., Rose, P., Barton, C., McCulloch, J., Berard, B., Moore, J.M., Petty, S., Spielman, P., 2003. In Situ Stress, Fracture and Fluid Flow Analysis—East Flank of the Coso Geothermal Field. In Proceedings of the twenty-eighth workshop on geothermal reservoir engineering, Stanford University, Stanford, CA, USA, pp. 34-49.

Sippel, R. F., Glover, E. D., 1965. Structures in Carbonate Rocks made Visible by Luminescence Petrography. Science, Vol. 150, No. 3701, pp. 1283-1287.

Slater, C., Preston, T., Weaver, L. T., 2001. Stable Isotopes and the International System of Units. Rapid Communications in Mass Spectrometry, Vol.15, No.15, pp. 1270-1273.

Sparkman, O. D., 2000. Mass Spectrometry Desk Reference. Journal of the American Society for Mass Spectrometry, Pittsburgh, PA, Global View Publishing.

Swanson, E. M., Wernicke, B. P., Eiler, J. M., Losh, S., 2012. Temperatures and Fluids on Faults based on Carbonate Clumped–Isotope Thermometry. American Journal of Science, Vol. 312, No. 1, pp. 1-21.

Wyld, S. J., 2002. Structural Evolution of a Mesozoic Backarc Fold-and-Thrust Belt in the US Cordillera: New Evidence from Northern Nevada. Geological Society of America Bulletin, Vol. 114, No. 11, pp. 1452-1468.

Yasuhara, H., Polak, A., Mitani, Y., Grader, A. S., Halleck, P. M., Elsworth, D., 2006. Evolution of Fracture Permeability through Fluid–Rock Reaction under Hydrothermal Conditions. Earth and Planetary Science Letters, Vol. 244, No. 1, pp. 186-200.

Zheng, Y. F., Hoefs, J., 1993. Carbon and Oxygen Isotopic Covariations in Hydrothermal Calcites. Mineralium Deposita, Vol. 28, No.2, pp. 79-89.

Table 1: Sample List. This is a comprehensive list of all samples run with corresponding isotopic and clumped isotope values given. Sample ID's are established as follows: (Well Area)-(Well Depth)-(Sample Run #).

Sample	$\delta^{13}C$ (‰), (VPDB)	$\delta^{13}C$ (‰), Stnd error	$\delta^{18}O_{carb}$ (‰), (VPDB)	$\delta^{18}O_{carb}$ (‰), Stnd error	$\delta^{18}O_{H2O}$ (‰), (VSMOW)	$\delta^{18}O_{H2O}$ (‰), Stnd error	Δ_{47} (‰) ARF	$T(\Delta_{47})$ (°C) Passey & Henkes	$T(\Delta_{47})$ Stnd error	$T(\Delta_{47})$ (°C) Stnd Dev
26A14-1680-2	-8.1	0.03	-32.8	0.07						
26A14-1990-1	-7.0	0.03	-19.6	0.07						
26A14-1990-2	-9.3	0.03	-25.4	0.07						
26A14-2110-1	-7.3	0.03	-27.6	0.07						
26A14-2110-2	-7.5	0.03	-32.2	0.07						
26A14-2600-2	-7.0	0.03	-32.4	0.12						
26A14-2600-FG	-13.4	0.05	-13.2	0.12	-12.1	0.6	0.711	18.705	0.007	0.014
3423-3320-2	-7.9	0.03	-26.0	0.07						
3814-3000-1	-8.6	0.03	-34.8	0.07						
3814-3000-2	-7.8	0.03	-33.3	0.07						
3814-3090-1	-9.6	0.03	-34.0	0.07						
3814-3090-2	-10.8	0.03	-25.5	0.07						
4127-4700	-7.4	0.03	-21.0	0.12	-1.1	0.6	0.459	148.578	0.005	0.008
4127-4700-1	-6.7	0.03	-24.1	0.07						
4127-4700-2	-7.2	0.03	-16.2	0.07						
4127-5760-1	-5.6	0.03	-14.3	0.07						
4127-5760-2	-6.8	0.03	-25.7	0.07						
4127-6140-1	-7.3	0.03	-27.7	0.07						
4127-6140-2	-8.0	0.03	-28.6	0.07						
4127-6140	-8.2	0.19	-27.3	0.43	-9.3	2.8	0.479	131.823	0.027	0.039
4127-7690-1	-6.5	0.03	-23.3	0.12						
4127-7690-2	-6.0	0.03	-24.5	0.12						
5815-4450-1	-8.3	0.07	-24.1	0.01						
5815-4450-2	-8.2	0.03	-15.2	0.12						
5815-4930-1	-7.9	0.03	-27.4	0.07						
5815-4930-2	-5.1	0.03	-25.5	0.07						
5815-5360-2	-6.1	0.03	-29.0	0.12						
5815-5570-1	-8.3	0.03	-35.3	0.12						
5815-5570-2	-9.0	0.03	-34.2	0.12						
5815-5570	-7.4	0.01	-30.4	0.03	-13.3	2.7	0.489	124.194	0.032	0.045
6122-3920-1	-7.0	0.03	-24.0	0.12						
6122-3920-2	-6.9	0.03	-23.9	0.12						
6122-4010-1	-6.8	0.03	-23.8	0.12						

Sample	$\delta^{13}C$ (‰), (VPDB)	$\delta^{13}C$ (‰), Stnd error	$\delta^{18}O_{carb}$ (‰), (VPDB)	$\delta^{18}O_{carb}$ (‰), Stnd error	$\delta^{18}O_{H2O}$ (‰), (VSMOW)	$\delta^{18}O_{H2O}$ (‰), Stnd error	Δ_{47} (‰) ARF	$T(\Delta_{47})$ (°C) Passey & Henkes	$T(\Delta_{47})$ Stnd error	$T(\Delta_{47})$ (°C) Stnd Dev
6122-4980-1	-9.0	0.03	-30.4	0.12						
6122-4980-2	-6.7	0.03	-28.0	0.12						
6122-5510-2	-8.5	0.03	-35.8	0.12						
8622-3610-1	-7.0	0.03	-19.4	0.07						
8622-3610-2	-7.1	0.03	-21.3	0.07						
8622-3610	-7.2	0.04	-21.9	0.04	-2.0	1.4	0.459	148.578	0.015	0.021
8622-4580-1	-10.1	0.03	-30.1	0.07						
8622-4580-2	-9.7	0.03	-29.7	0.07						
8911-2020-1	-7.2	0.03	-29.3	0.12						
8911-2020-2	-7.9	0.03	-30.3	0.12						
9115-4310-1	-8.2	0.03	-29.6	0.07						
9115-4310-2	-6.7	0.03	-26.3	0.07						
9115-4590-1	-7.6	0.03	-29.0	0.07						
9115-4590-2	-7.9	0.03	-32.0	0.07						
9115-4840-1	-8.6	0.03	-32.1	0.12						
9115-4840-2	-7.3	0.03	-29.4	0.12						
9115-6690-1	-6.8	0.03	-27.5	0.07						
9115-6690-2	-7.4	0.03	-20.0	0.07						
1-1960-1	-7.7	0.07	-31.8	0.01						
1-1960-2	-7.9	0.07	-32.1	0.01						
1-1960	-7.9	0.01	-32.2	0.05	-11.3	2.7	0.445	161.724	0.028	0.040
2-720-FG	-7.2	0.01	-29.6	0.01	-9.9	0.6	0.460	147.687	0.007	0.009
2-1583-1	-7.5	0.07	-33.5	0.01						
2-1583-2	-7.4	0.07	-33.4	0.01						
2-1583	-7.4	0.06	-33.5	0.07	-13.3	0.7	0.453	154.053	0.006	0.009
2-2806-1	-9.2	0.07	-24.6	0.01						
2-2806-2	-9.2	0.07	-24.5	0.01						
2-3456-2	-11.8	0.07	-25.2	0.01						
2-3456	-11.7	0.01	-25.8	0.08	0.7	1.4	0.393	226.063	0.011	0.016
2-4607-1	-12.3	0.07	-24.5	0.01						
2-4607-2	-12.3	0.07	-22.5	0.01						

Figures

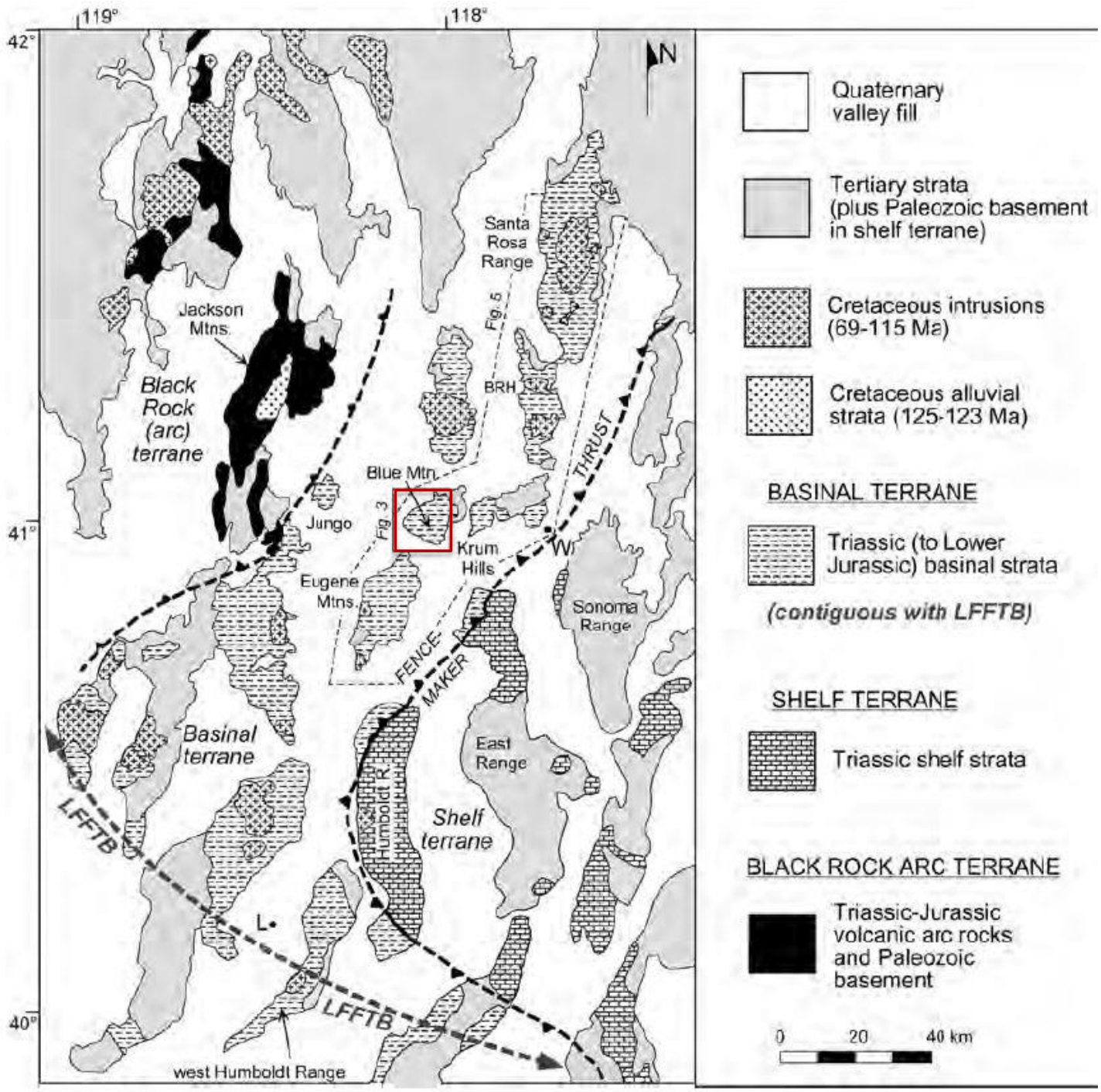

Figure 1. Blue Mountain in northern Nevada sits at the northern end of the Luning-Fencemaker fold-and-thrust belt. Figure courtesy of Wyld, 2002.

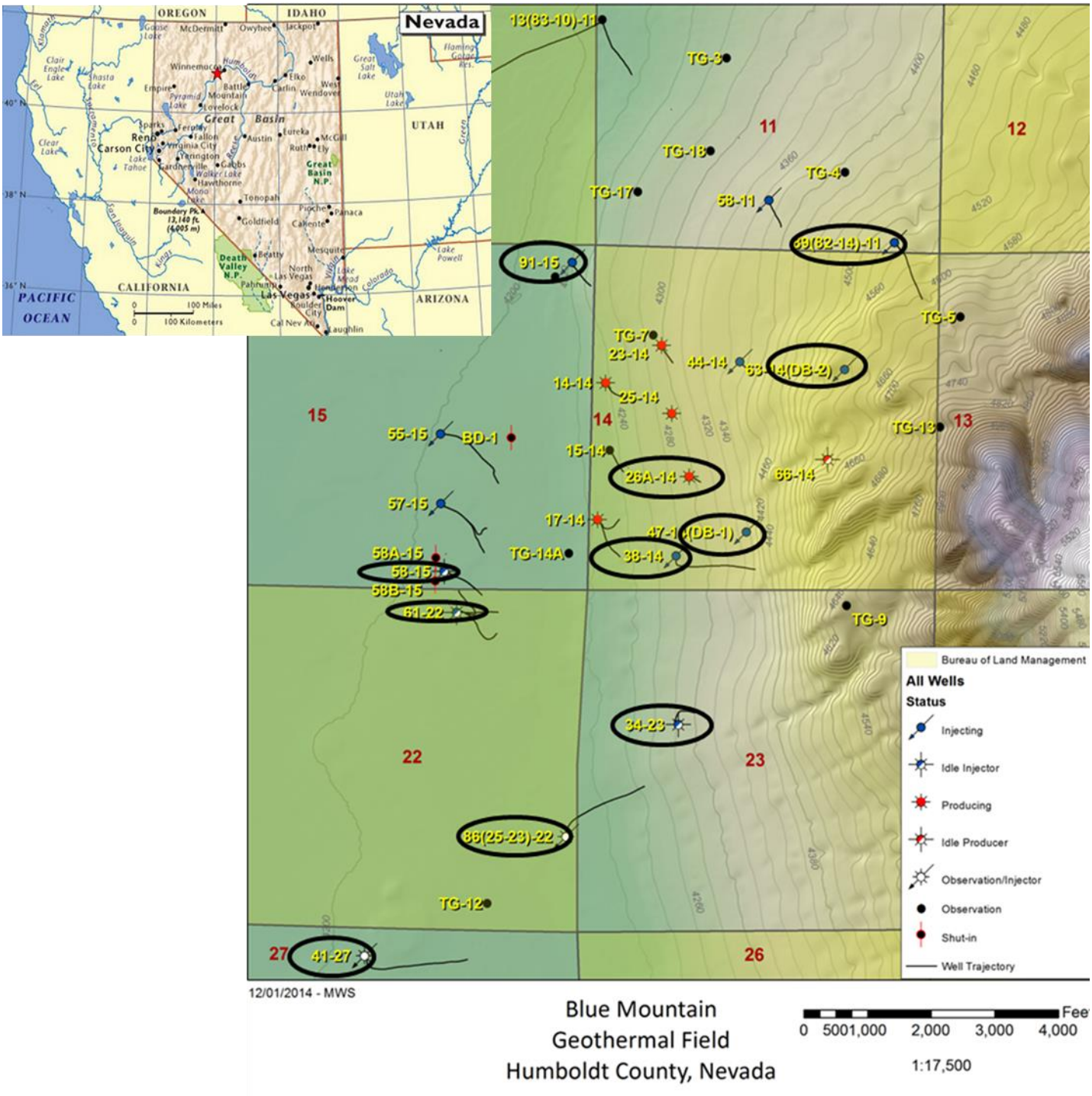

Figure 2. Blue Mountain geothermal field. Wells that were selected for evaluation are circled. Geothermal reservoir map courtesy of Mike Swyer, AltaRock Energy. Nevada state map courtesy of greatdreams.com.

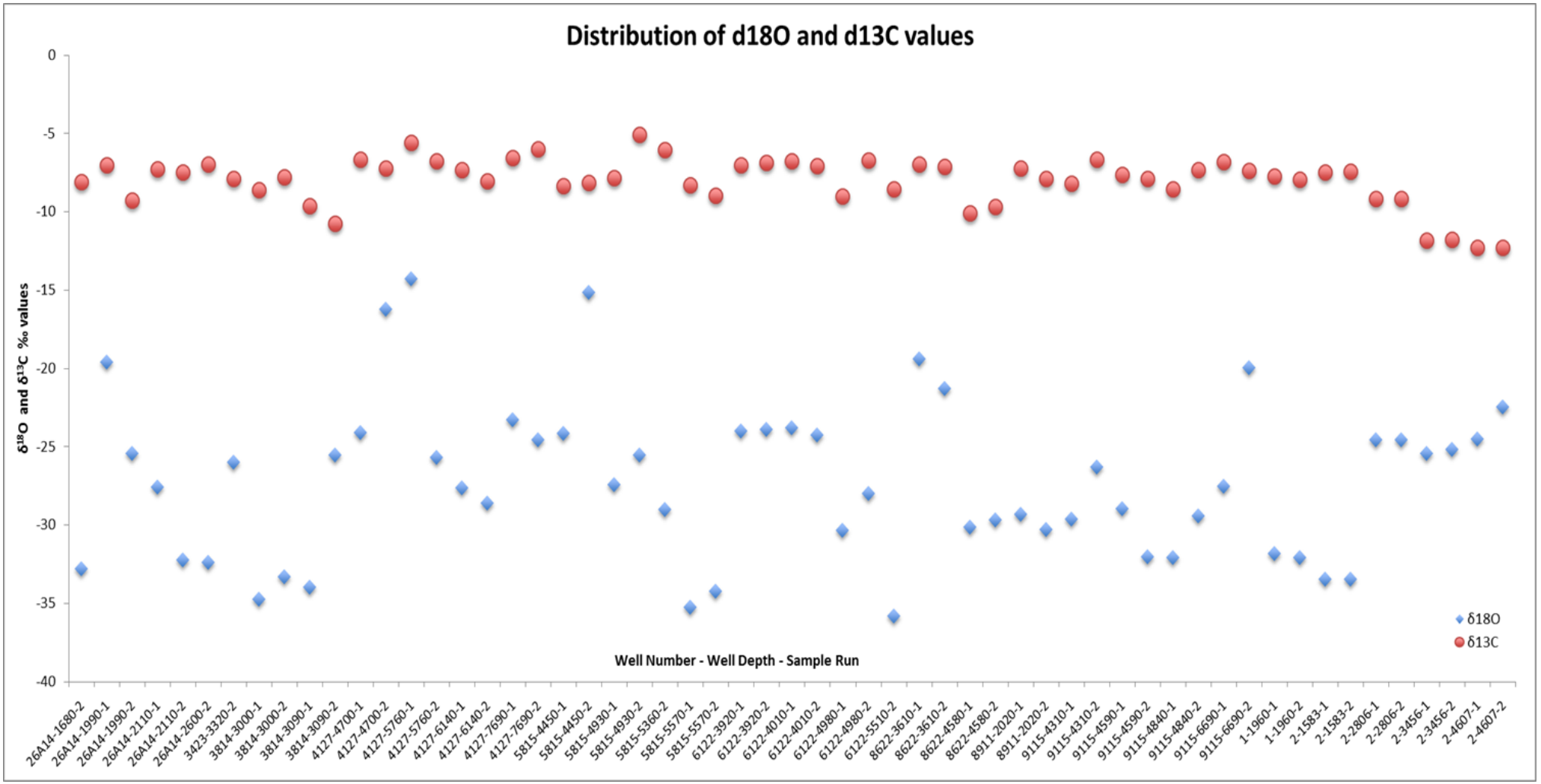

Figure 3. Graph shows the stable isotope values for the seventy-two samples taken from eleven wells of both cuttings and core. There is significant variability in $\delta^{13}O$ values.

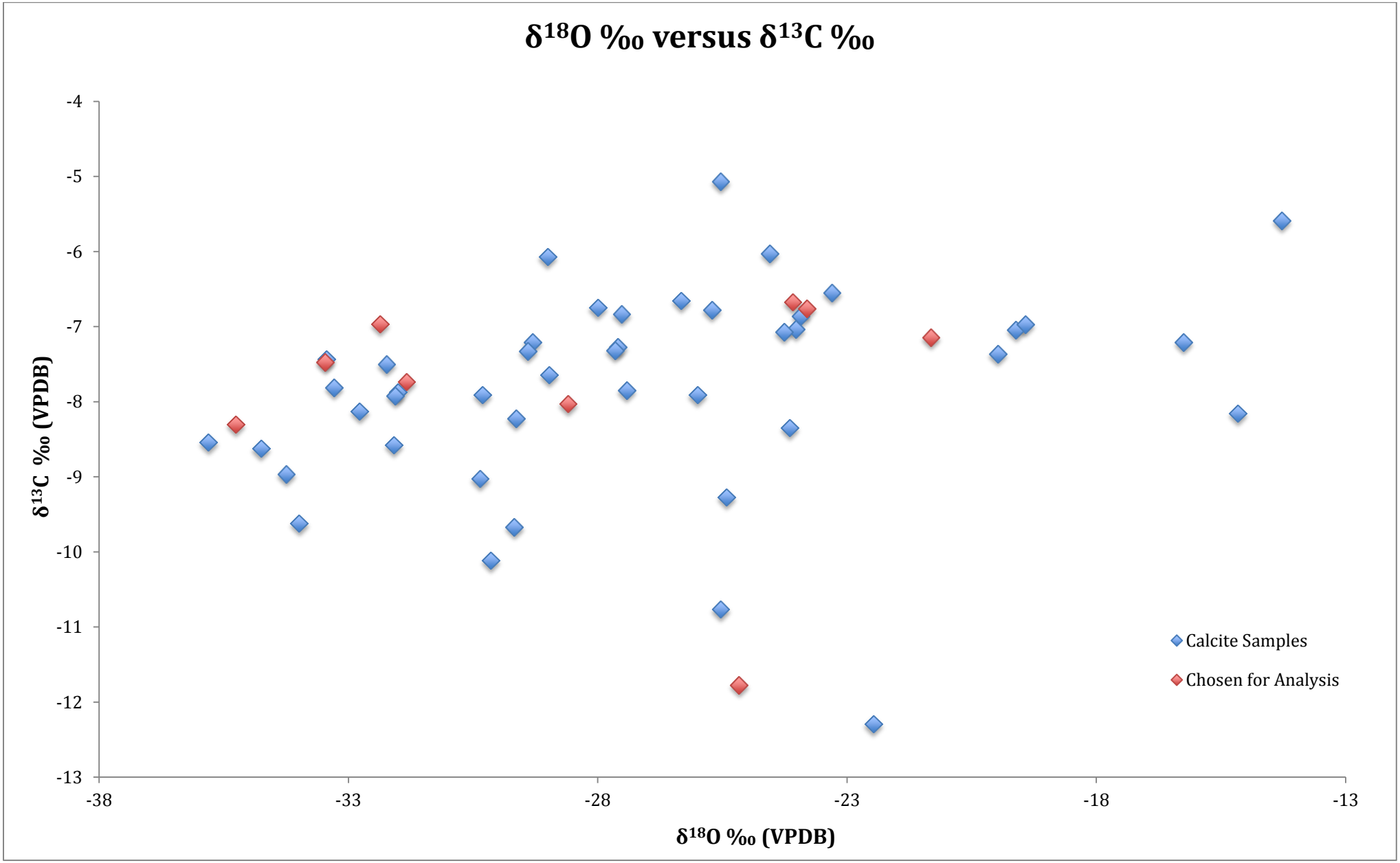

Figure 4. Graph of $\delta^{18}O_{carbonate}$ versus $\delta^{13}C_{carbonate}$ in which the subset of ten samples was chosen. I attempted to vary my choices throughout the dataset.

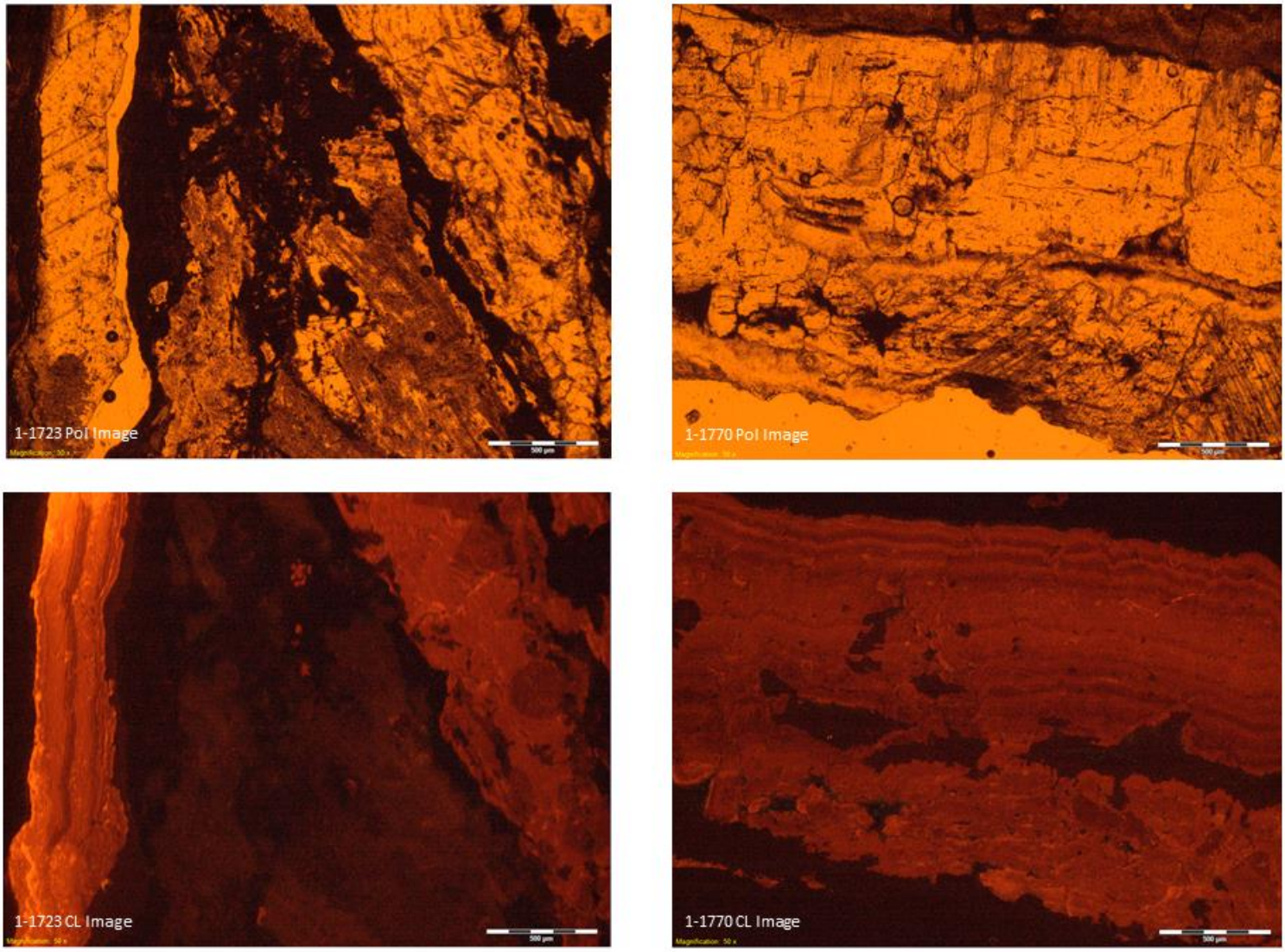

Figure 5. Transmitted light images (top) for well DB-1 at depths 1723’ and 1770’. The polarized images show twinning. The CL images (bottom) show reddish orange luminescence, as well as high and low intensity contrasting bands.

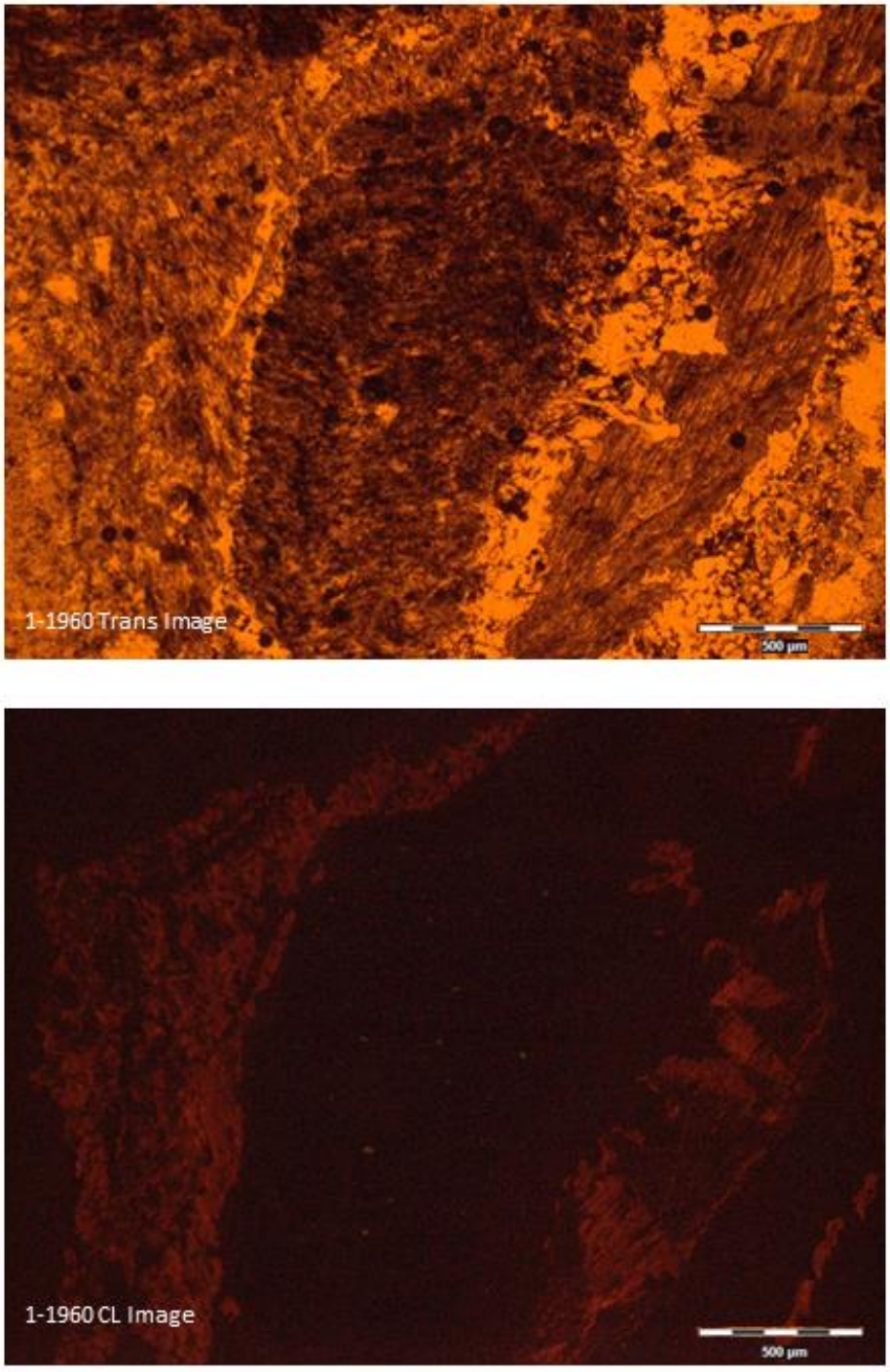

Figure 6. Polarized image (top) for well DB-1 at depth 1960'.The CL image (bottom) show reddish orange luminescence of fracture filling calcite.

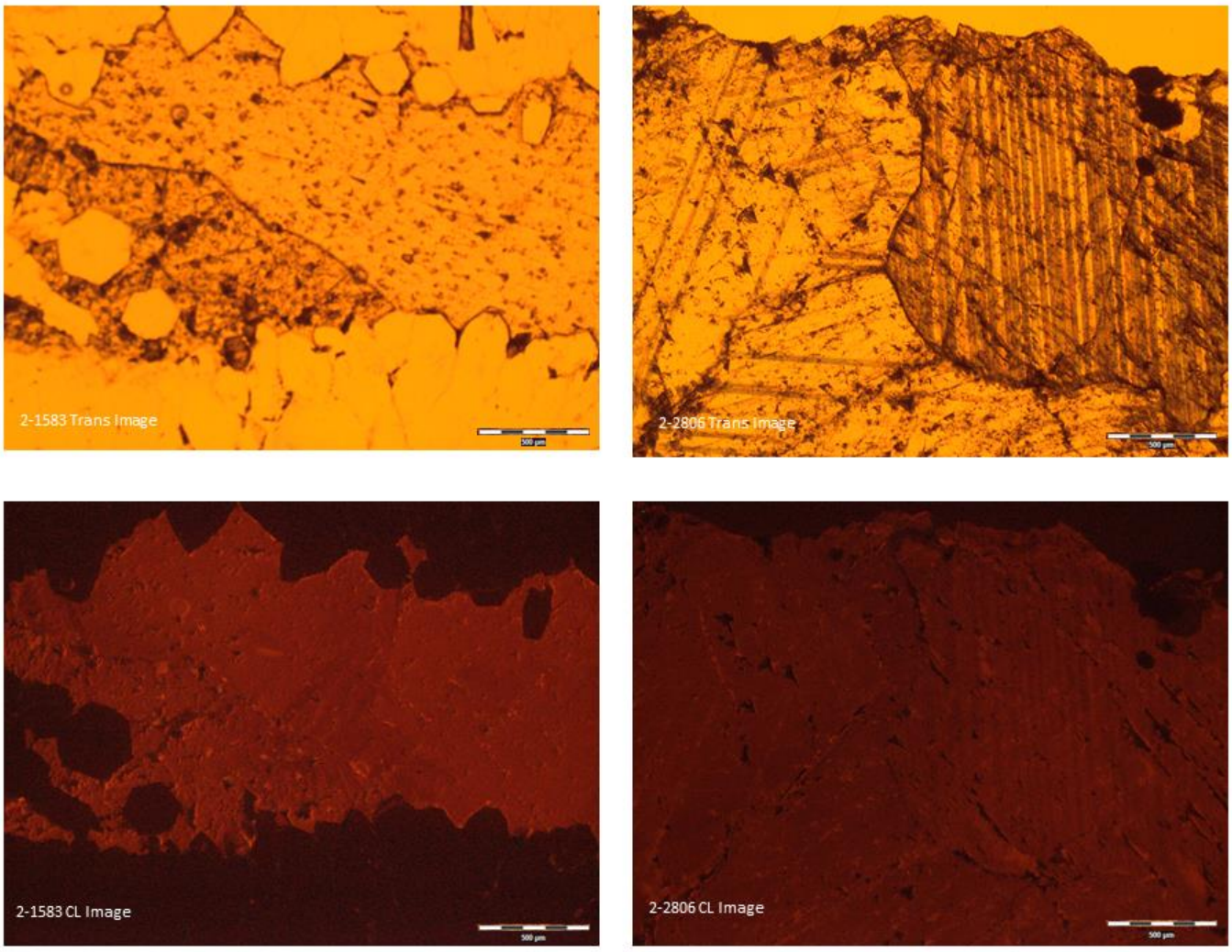

Figure 7. Transmitted light images (top) for well DB-2 at depths 1583’ and 2806’. The transmitted light images show twinning, which is seen as striping. The CL images (bottom) show reddish orange luminescence of fracture fill calcite.

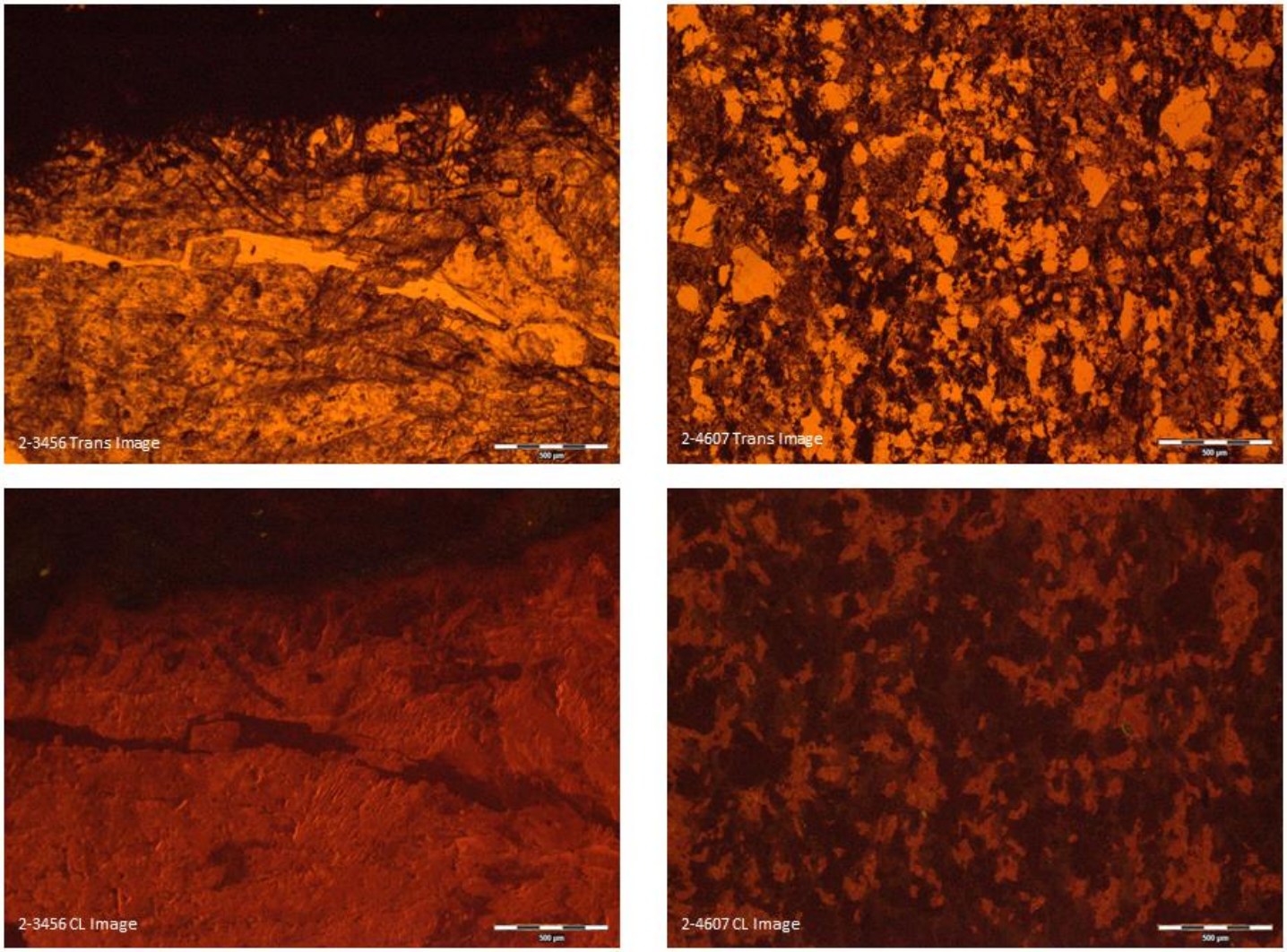

Figure 8. Transmitted light images (top) for well DB-2 at depths 3456’ and 4607’. The CL images (bottom) show reddish orange luminescence of fracture fill calcite.

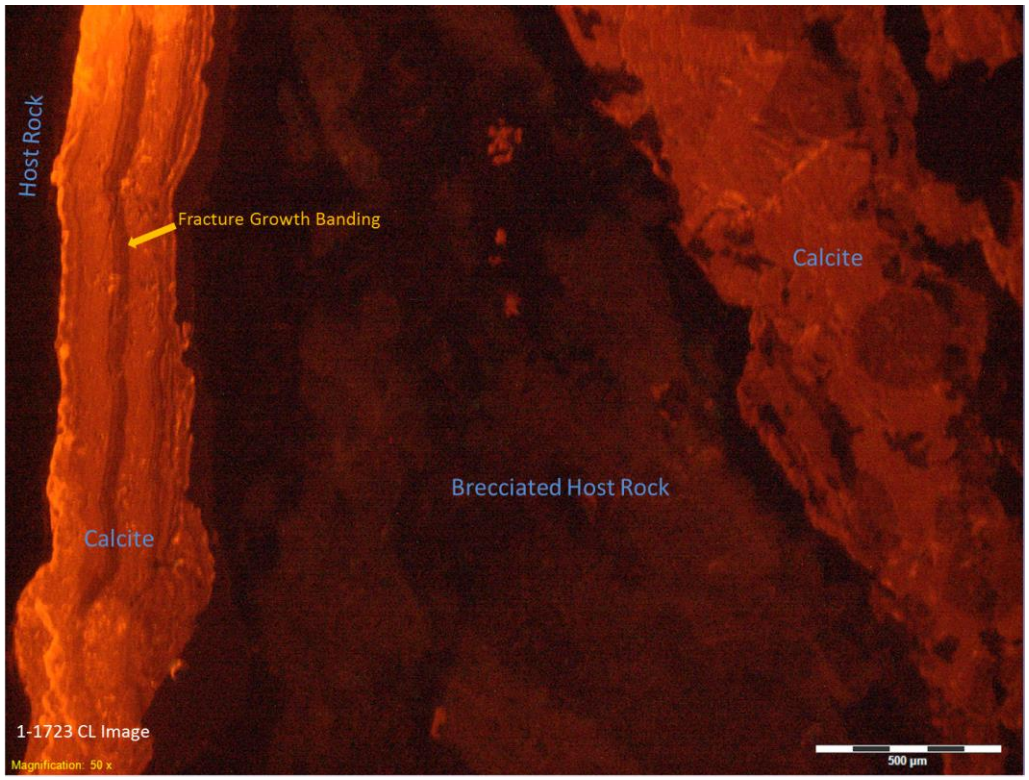

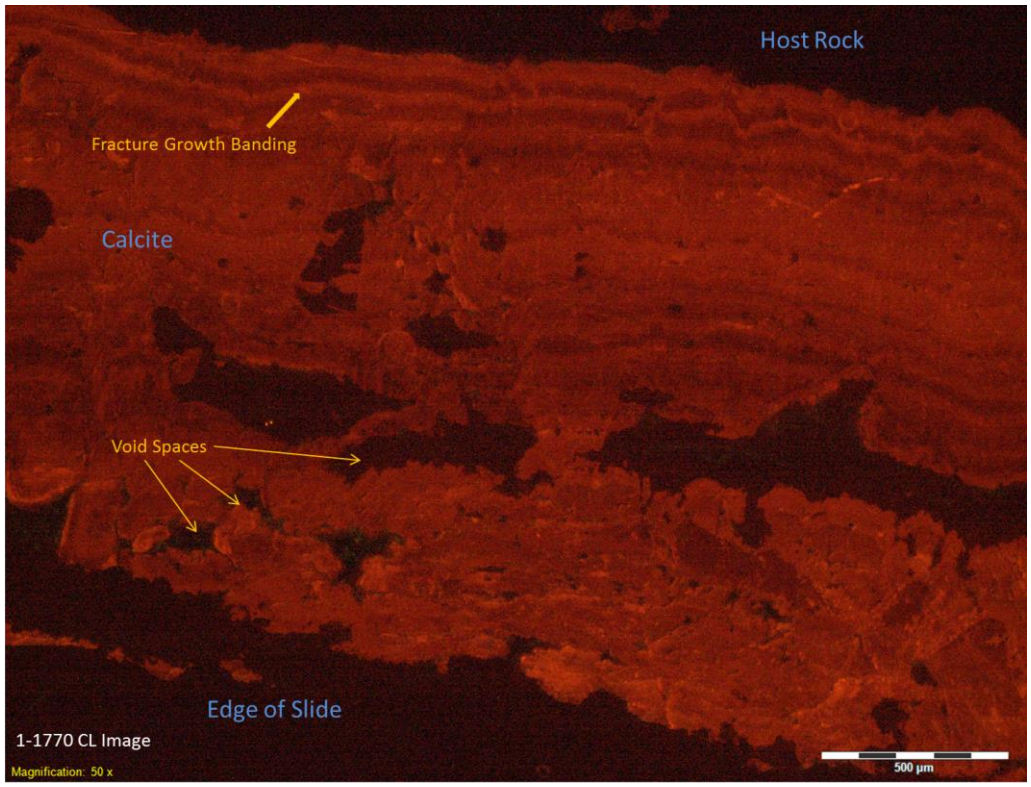

Figure 9. CL images from core DB-1 at 1723’ and 1770’ depth. Fracture growth banding can also be seen in the upper portion of the image as higher and lower luminescence intensities. The dark spots are predominantly voids.

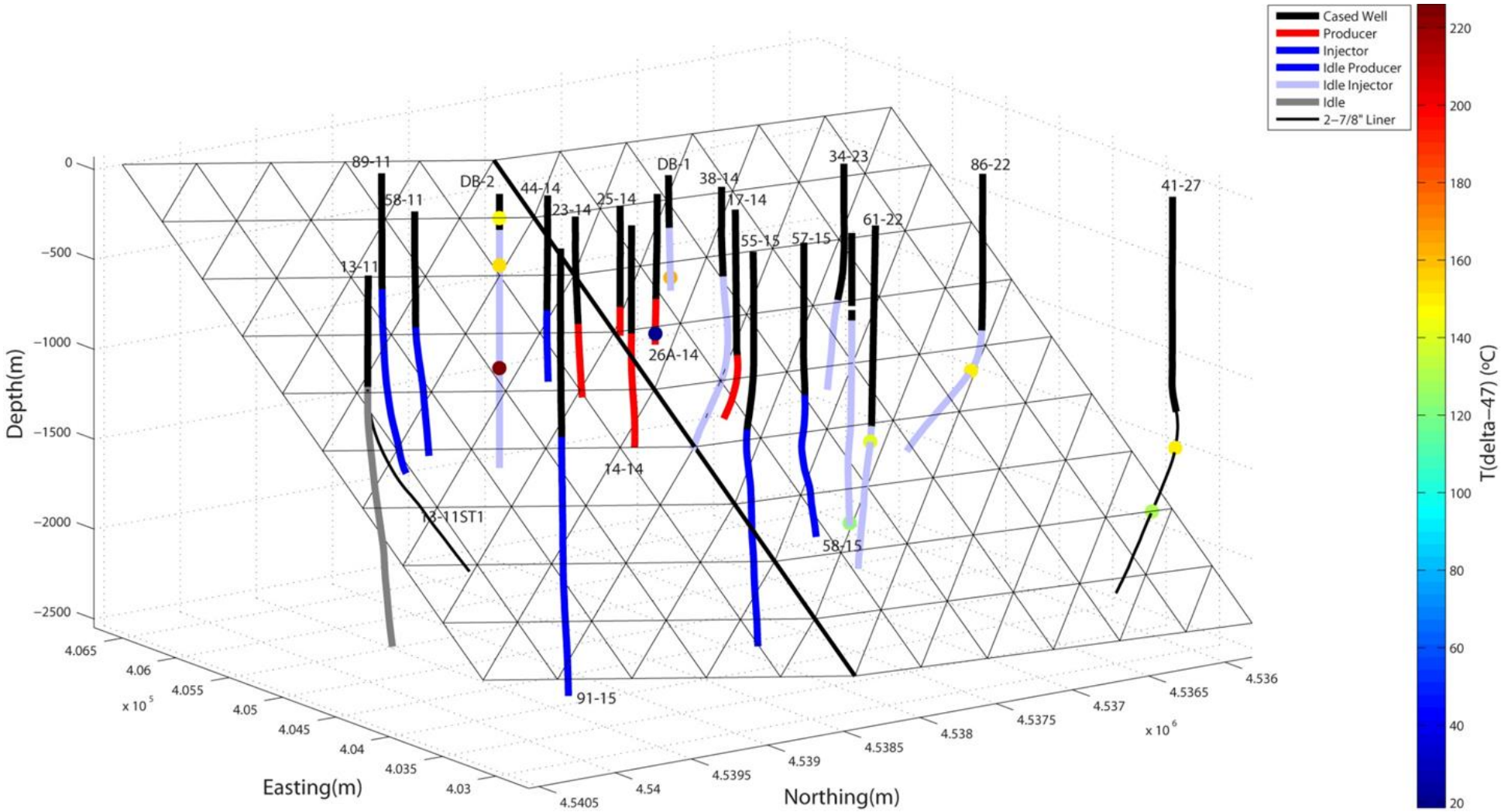

Figure 10. Three dimensional graph of the geothermal well field. Clumped isotope data points are marked as colored circles and placed at the sampled depths. The circles are color coded to indicate temperature. There are two planes that the wells are intersecting, which are faults. The wells change from black to a color where they intercept the fault.

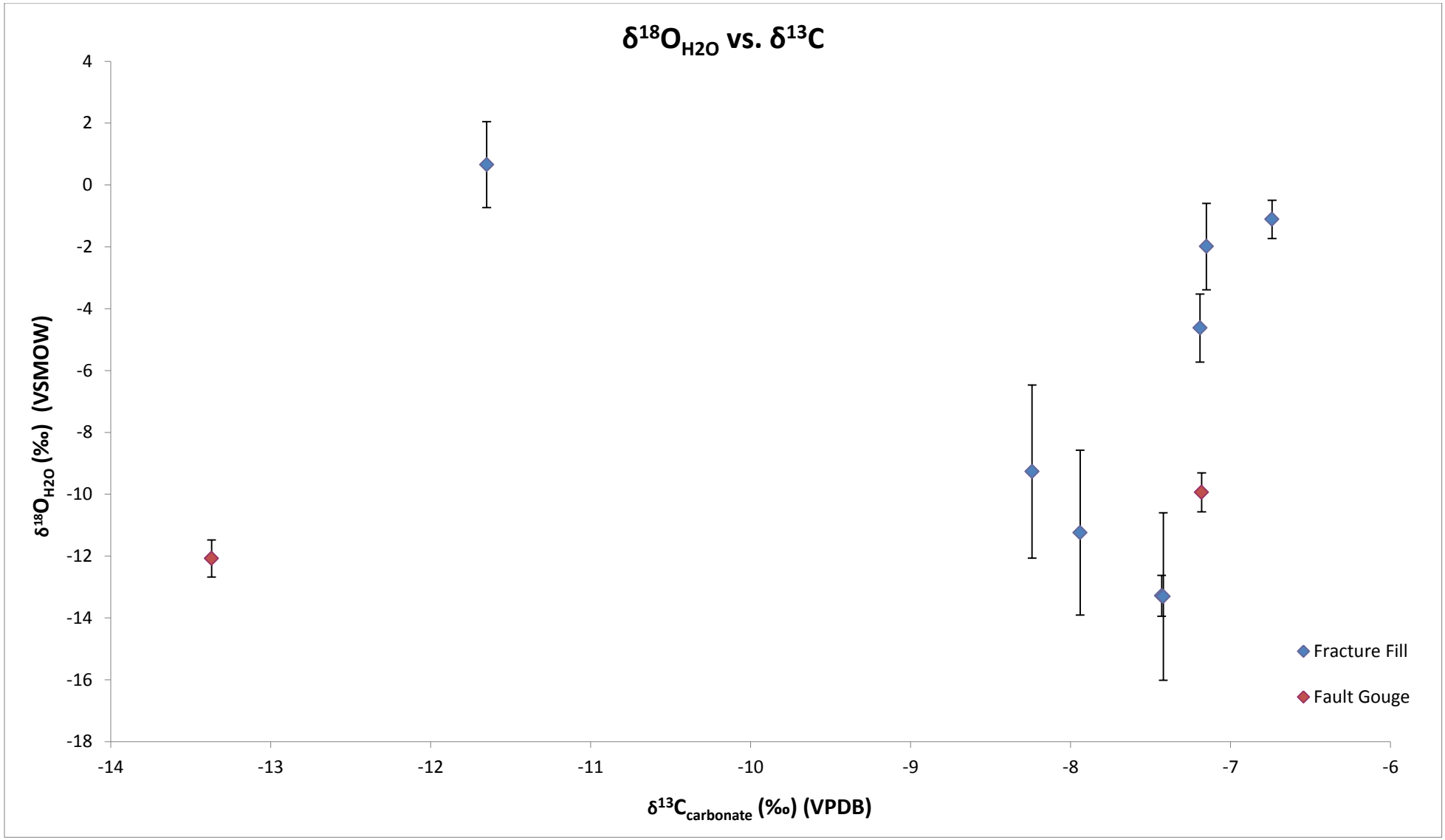

Figure 11. We generally have a relatively narrow range for our $\delta^{13}C_{carbonate}$ values, but samples have a wide variety of values for $\delta^{18}O_{H2O}$. The two $\delta^{13}C_{carbonate}$ extremes reflect the two temperature extremes of the dataset.

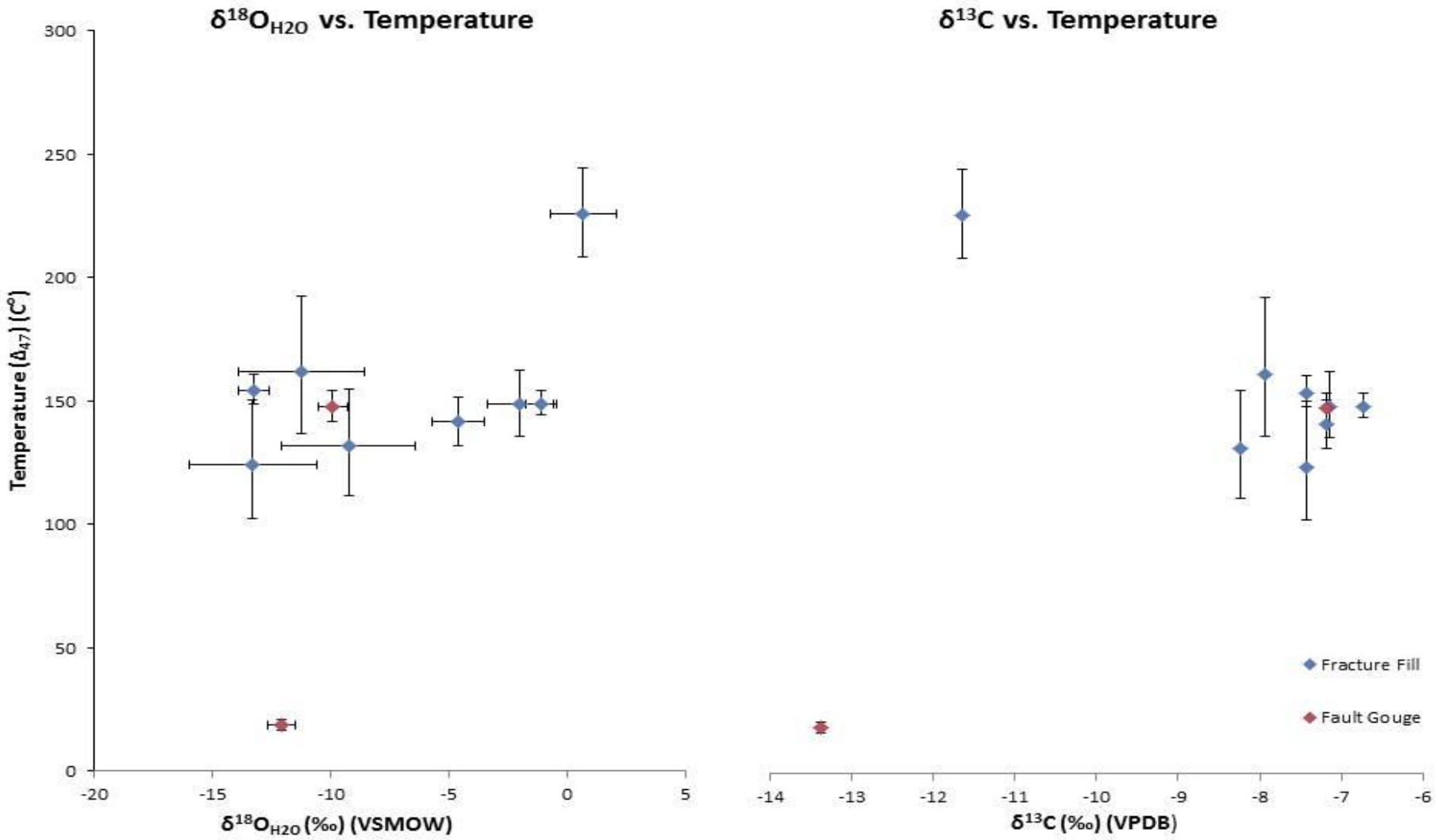

Figure 12. The $\delta\,^{18}O_{H2O}$ and $\delta\,^{13}C_{carbonate}$ values show very little variation with temperature. The two outliers reflect the temperature extremes for our system.

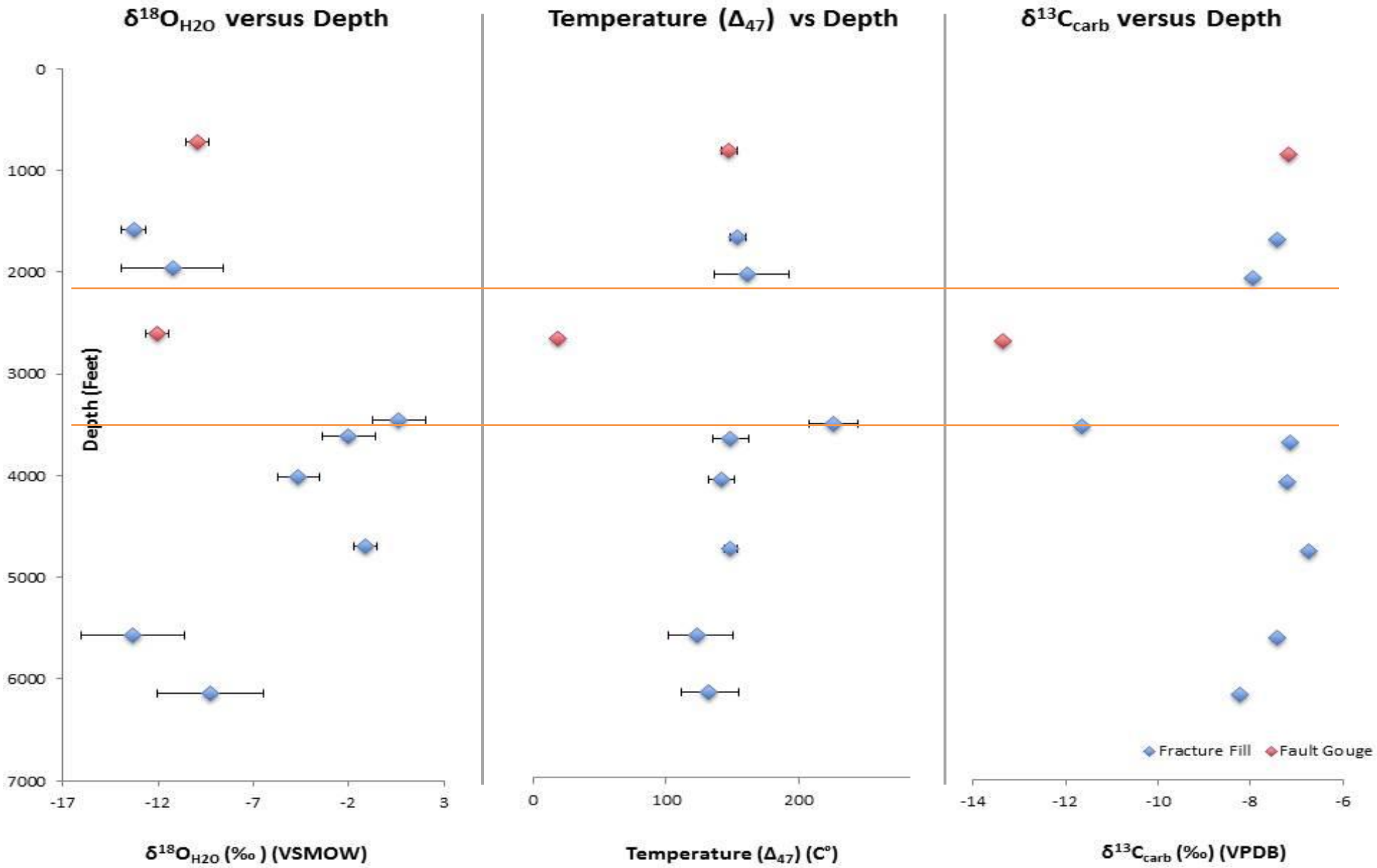

Figure 13. $\delta^{18}O_{H2O}$, $\delta^{13}C_{Carb}$, and temperature relationship with depth. There is a pattern viewed across the stable isotope and temperature data at a depth interval between 2100 feet to 3500 feet (noted on graph between orange lines). For the cold temperature sample, this depth marks a fault cutting across the geothermal field.